Journal of Alloys and Compounds 509 (2011) 7794–7797

Contents lists available at ScienceDirect

Journal of Alloys and Compounds

journal homepage: www.elsevier.com/locate/jallcom

Infrared emission properties and energy transfer in ZnO–SiO_2:Yb^{3+} composites

F. Xiao[a,b], R. Chen[b], Y.Q. Shen[c], B. Liu[b], G.G. Gurzadyan[b], Z.L. Dong[c], Q.Y. Zhang[a,*], H.D. Sun[b,*]

[a] MOE Key Lab of Specially Functional Materials and Institute of Optical Communication Materials, South China University of Technology, Guangzhou 510641, PR China
[b] Division of Physics and Applied Physics, School of Physical and Mathematical Sciences, Nanyang Technological University, Singapore 639798, Singapore
[c] Division of Materials Science, School of Materials Science and Engineering, Nanyang Technological University, Singapore 639798, Singapore

ARTICLE INFO

Article history:
Received 17 March 2011
Received in revised form 1 May 2011
Accepted 4 May 2011
Available online 10 May 2011

Keywords:
Photoluminescence
Energy transfer
Quantum dots
Solar cell

ABSTRACT

Intense near-infrared emission at 1 μm has been obtained in ZnO–SiO_2:Yb^{3+} composites via a facile sol–gel method upon broadband ultraviolet light excitation. Systematic optical measurements including static and time-resolved photoluminescence have been performed to elucidate the energy transfer from ZnO quantum dots to Yb^{3+} ions. The dependence of energy transfer efficiency on Yb^{3+} concentration has been investigated in detail. Codoping with Li^+ ions leads to about twice enhancement of the near-infrared luminescence intensity around 1 μm at room temperature. The enhancement in the luminescence intensity could be mostly attributed to the modification of the local symmetry around Yb^{3+} ions by codoping with Li^+ ions.

1. Introduction

The ever-increasing demand for energy as well as the dwindling fossil fuels resources has been calling for the establishment of a clean and sustainable energy system [1]. Photovoltaic cells play the bridge role which directly converts the green solar energy into clean electrical energy via photovoltaic effect [2]. The state-of-the-art commercial *c*-Si solar cells operate with energy conversion efficiencies of around 15%, which is still much lower than the Shockley–Queisser efficiency limit of 30% [3]. One of the major energy loss mechanisms leading to the low energy conversion efficiency of solar cells is the carrier thermalization generated by the absorption of high-energy photons. To reduce this part of energy loss, one of the most effective methods is to modify the solar spectrum through down-converting the high-energy photons [4,5]. The down-conversion (DC) luminescent materials based on rare-earth ions have been widely investigated as a potential DC luminescent converter in front of *c*-Si solar cell panels to reduce thermalization losses [5–9]. However, the forbidden *f*–*f* transition of rare-earth ions lead to narrow absorption in the UV-blue region, which restricts their practical applications [10].

ZnO, a direct band gap semiconductor, is considered as an attractive donor in the process of efficiently transferring energy into the rare-earth ions (e.g. Eu^{3+}, Dy^{3+}, Ce^{3+}), which has been widely applied in display and optoelectronic devices [11–16]. To make full use of the UV-blue region of solar spectrum, we propose ZnO–SiO_2:Yb^{3+} hybrid materials as potential luminescent candidates to enhance the photo response of the silicon-based solar cells. Herein, we demonstrate energy transfer (ET) process from ZnO quantum dots (QDs) to Yb^{3+} embedded in SiO_2 matrix. Based on static and dynamic spectroscopic data, the energy transfer mechanism leading to the conversion of broad UV-blue emission to NIR photons will be discussed in detail. Highly enhanced emission around 1 μm due to codoping with Li^+ ions has also been investigated.

2. Experimental details

A series of ZnO–SiO_2:*x*%Yb^{3+} composites doped with and without Li^+ ions were prepared by a facile sol–gel method. In brief, 1 mmol zinc acetate-2-hydrate [$Zn(CH_3COOH)_2{\cdot}2H_2O$; Sigma–Aldrich, 99.999%] and LiOH (for the sample doped with Li^+) was dissolved in the mixture of moderate ethanolamine ($NH_2CH_2CH_2OH$) and absolute ethanol (analytical reagent) with constantly stirring at 65 °C. Meanwhile, 9 mmol ethylorthosilicate (TEOS), ethanol, distilled water and different amount of ytterbium nitric acid (*x* = 0, 1, 3, 5, 7, 10 mol.%) were mixed followed by stirring for several hours at room temperature. Then the above two solutions were mixed together and stirred for 4 h. The transparent gels were obtained after aged at room temperature for one week and subsequently dried at 60 °C for several days. Finally, the as-prepared bulk samples were calcinated at 550 °C for 2 h. This heat treatment process stimulates the nucleation and growth of ZnO QDs.

The high resolution transmission electron microscopy (HRTEM) images were taken by using a JEOL JEM-2100F microscope (C_s = 0.5 mm, accelerating voltage = 200 kV). The photoluminescence (PL) and photoluminescence excitation (PLE) of the undoped sample were characterized on a Shimadzu RF-5301PC spectrophotometer equipped with a 150 W Xenon lamp as the excitation source at room temperature. The PL spectra were also detected using the 325 nm line from a continuous-wave He–Cd laser as excitation source, the UV emission was recorded by a photomultiplier and the NIR emission from Yb^{3+} ions was detected by a Peltier cooled InGaAs photodiode using standard lock-in amplifier technique.

* Corresponding author. Tel.: +86 20 87113681.
E-mail addresses: qyzhang@scut.edu.cn (Q.Y. Zhang), hdsun@ntu.edu.sg (H.D. Sun).

0925-8388/$ – see front matter © 2011 Elsevier B.V. All rights reserved.
doi:10.1016/j.jallcom.2011.05.011

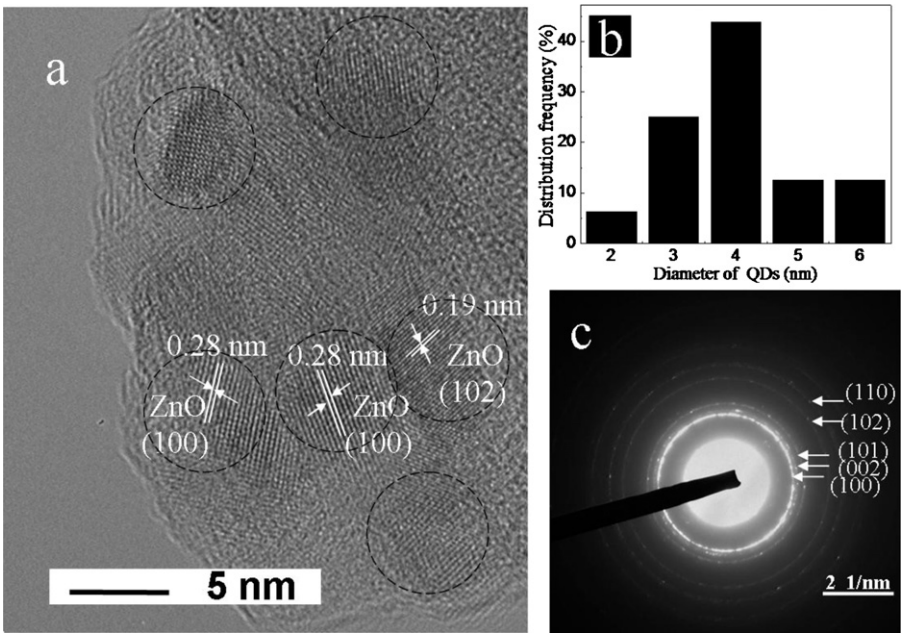

Fig. 1. (a) HRTEM image of the ZnO QDs precipitated in SiO_2 matrix, (b) the size distribution histogram of ZnO QDs, (c) the electron diffraction pattern of the present region.

The low temperature PL measurements were performed by using a closed cycle helium cryostat. Time-resolved PL (TRPL) was carried out at room temperature by time-correlated single photon counting (TCSPC) technique, with a resolution of 10 ps (PicoQuant PicoHarp 300), while a pulse laser (100 fs, 80 MHz) with wavelength of 280 nm from the third harmonic generation of a Titanium sapphire laser (Chameleon, Coherent Inc.) was used as an excitation source.

3. Results and discussions

The HRTEM image of ZnO–SiO_2 composites and the corresponding size distribution histogram of ZnO QDs are shown in Fig. 1(a) and (b), respectively. It is clearly demonstrated that highly crystalline ZnO QDs with size ranging from 2 to 6 nm were dispersed homogeneously in the host matrix. The mean diameter is about 4 nm. Lattice fringes were also clearly shown from different single ZnO QDs, which indicates that the selected thermal treatment temperature is appropriate for the crystallization of ZnO. The distances between lattice fringes are about 2.8 and 1.9 Å, corresponding to (1 0 0) and (1 0 2) lattice planes of wurtzite ZnO structure, respectively [17]. The electron diffraction pattern was taken from the area in Fig. 1(a) and presented in Fig. 1(c), showing the diffraction rings of (1 0 0), (0 0 2), (1 0 1), (1 0 2) and (1 1 0) in good agreement with those of wurtzite ZnO.

Fig. 2(a) presents the PL and PLE spectra of ZnO QDs dispersed in SiO_2 matrix without Yb^{3+} doping. The PLE spectrum shows a broadband absorption extending from 250 to 380 nm with peak wavelength at 340 nm (3.65 eV) [18,19]. Upon 340 nm excitation, the PL spectrum displays a near UV emission band centered at 397 nm which should originate from some defects states related to oxygen vacancies near the band edge of ZnO [20,21]. It should be mentioned that the ZnO–SiO_2 interface plays an important role in the UV emission of ZnO QDs. Due to the surface nature of the ZnO QDs, the photon-generated carriers can be trapped by these interface states, and then recombine and contribute to the UV emission [19]. However, the absence of the notable deep level green emission can be explained by the surface passivation of ZnO [22].

Fig. 2(b) shows the PL spectra of 10 ZnO–90 SiO_2 (in mol.%) composites with a varied content Yb^{3+} (0, 1%, 3%, 5%, 7%, and 10%) (in mol.%) under the 325 nm laser excitation. In addition to the UV emission at 397 nm originated from ZnO QDs, the NIR emission at around 1 μm originated from the $^2F_{5/2} \rightarrow {}^2F_{7/2}$ transition of Yb^{3+} ions can be clearly observed, and it is interesting to note that the emission intensity at 397 nm decreases monotonically with increasing Yb^{3+} content due to the enhanced ET from ZnO QDs to Yb^{3+} in SiO_2 matrix. Meanwhile, the intensity of NIR emission at around 1 μm increasing with the increase of Yb^{3+} concentrations

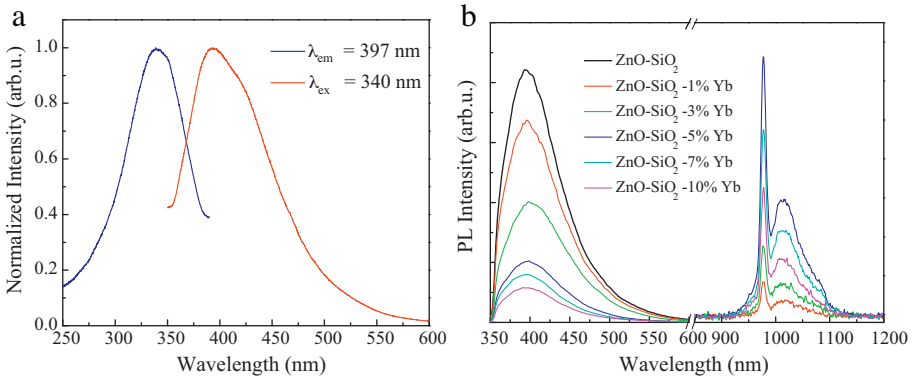

Fig. 2. PL and PLE spectra of (a) ZnO–SiO_2 based composite, (b) ZnO–SiO_2:Yb^{3+} composites with different Yb^{3+} concentration.

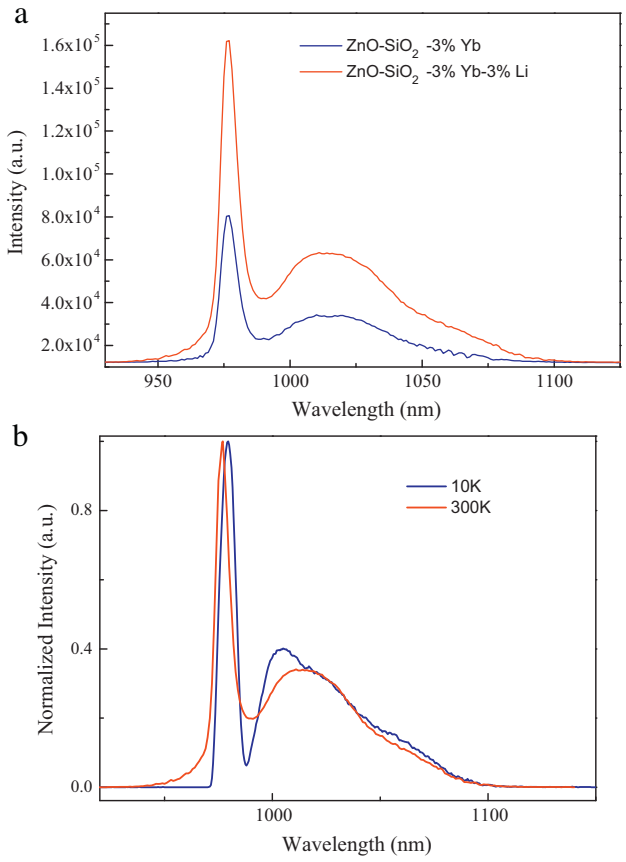

Fig. 3. (a) PL spectra of 3% Yb doped ZnO–SiO_2 composites without and with 3% Li contents (at room temperature), (b) PL spectra of ZnO–SiO_2-3% Yb, 3% Li (at 10 K and 300 K).

ranging from 1 mol.% to 5 mol.%, and then decreasing at the higher concentrations beyond 5 mol.%. This saturation phenomenon of the emission intensity of Yb^{3+} could be ascribed to the concentration quenching effect [23].

Fig. 3(a) shows the fluorescence spectra of Yb^{3+} ions doped ZnO QDs with and without the addition of 3 mol.% Li^+ ions measured at room temperature. With the Li^+ addition, it is clear that the PL intensity increased apparently and is about twice enhancement at 1 μm. It was suggested that the addition of charge compensators

Table 1
Decay lifetime for exponential components of *x*% Yb doped ZnO–SiO_2 composites excited at 280 nm with the emission monitored at 397 nm.

x (Yb mol.%)	τ_1 (ns)	A_1	τ_2 (ns)	A_2	τ^*_{eff} (ns)
x = 0	0.53647	5.49328	3.4039	0.75875	1.88
x = 1	0.48783	6.02938	3.3462	0.80126	1.85
x = 3	0.43296	8.87372	3.1681	0.80644	1.53
x = 5	0.35943	14.6516	3.0075	0.96314	1.26
x = 7	0.38665	13.0108	2.7715	0.85755	1.15
x = 10	0.33742	24.7709	2.7493	0.79278	0.84

of Li^+ ions will change the local structure of ZnO, which will lower the symmetry of the crystal field of Yb^{3+} ions and then result in the enhancement of PL intensity [24]. The comparison of PL spectra of Li^+ and Yb^{3+} doped ZnO–SiO_2 composites measured at 10 K and 300 K were shown in Fig. 3(b). Upon the excitation of 325 nm, the spectra are similar except the emission band at 10 K is sharper than at room temperature, which is attributed to the decrease of thermal line-broadening at low temperature.

In order to further confirm the ET from ZnO QDs to Yb^{3+} ions, TRPL measurements of the UV emission related to ZnO QDs were performed and the result is presented in Fig. 4(a). The TRPL data were obtained under 280 nm laser excitation and monitored at 397 nm. All of the decay curves exhibit multi-exponential feature and the corresponding luminescent decay times can be well fitted by a bi-exponential reconvolution as the form below,

$$I(t) = \int_{-\infty}^{t} \mathrm{IRF}(t') \sum_{i=1}^{2} A_i e^{-\frac{t-t'}{\tau_i}} dt' \quad (1)$$

where A_i is the amplitude of the *i*th component at time zero, τ_i is the corresponding decay time (luminescent lifetime), and IRF is the instrument response function. The curves plotted in (b) and (c) show the weighted residuals for the fitting of ZnO QDs with different contents. The straight lines indicate that the fitting is reliable.

The effective average lifetime of UV emission for ZnO QDs can be estimated by the following equation [25,26],

$$\tau^*_{eff} = \frac{A_1\tau_1^2 + A_2\tau_2^2}{A_1\tau_1 + A_2\tau_2} \quad (2)$$

The obtained values of A_1, A_2, τ_1, τ_2, and τ^*_{eff} are summarized in Table 1. For the sample without Yb^{3+} ions, the lifetime value was determined to be 1.88 ns. With increasing of the Yb^{3+} content, the lifetime of UV emission decreases from 1.85 to 0.84 ns, which provides a direct evidence for the ET from ZnO QDs to Yb^{3+} ions.

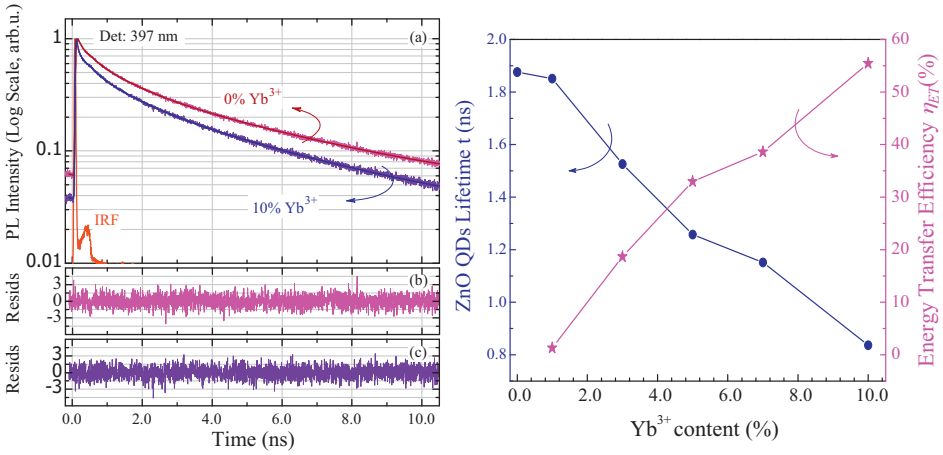

Fig. 4. (a) Luminescence decay curves recorded at 397 nm with the excitation of 280 nm laser for samples with different concentration of Yb^{3+}, (b) and (c) shows the weighted residuals during the reconvolution of 0 and 10 mol.% Yb^{3+}, respectively, (d) dependence of the Yb^{3+} content on the lifetime of ZnO QDs and ET efficiency from ZnO QDs to Yb^{3+}.

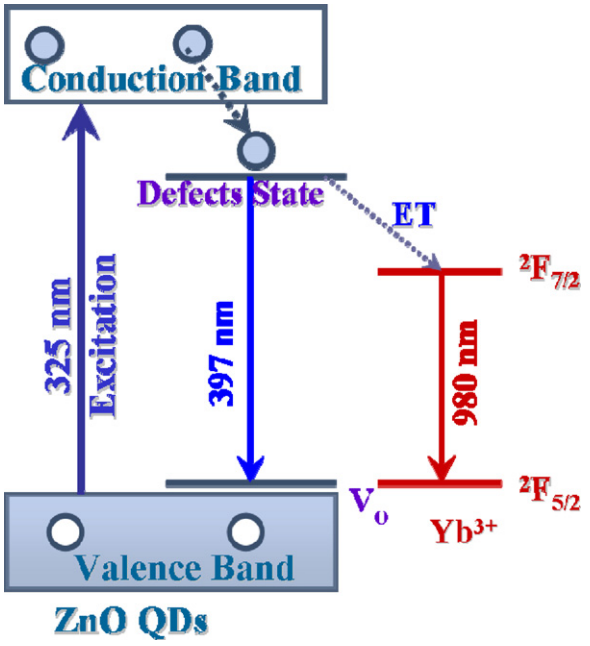

Fig. 5. Schematic energy level diagram of the ZnO–SiO_2 composites and Yb^{3+}, illustrating the mechanism of the ET for the UV and NIR emission.

The dependence of lifetime on the Yb^{3+} concentration was plotted in Fig. 4(d). From the decay curves, the ET efficiency (η_{ET}) of ZnO → Yb^{3+} can be determined by [7],

$$\eta_{ET} = 1 - \frac{\tau}{\tau_0} \quad (3)$$

where τ and τ_0 are the lifetimes of ZnO QDs with and without Yb^{3+} doping, respectively. From Fig. 4(d), it can be clearly observed that the ET efficiency (η_{ET}) increases gradually with increasing the Yb^{3+} dopant content and up to 55.42% when the Yb^{3+} concentration is equal to 10 mol.%. It was observed that there are some attached Yb_2O_3 nanoparticles around ZnO, and a little bit of Yb^{3+} ions can diffuse several tens of nanometer into ZnO lattice after the heat treatment process [27]. Furthermore, the formation of abundant silicon-oxytetrahedron may separates Yb^{3+} ions from the ZnO lattice which result in the relative low energy transfer efficiency from ZnO to Yb^{3+} ions.

The possible schematic energy transfer route was depicted by an energy-level diagram as shown in Fig. 5. Upon pumping from the valence band to the conduction band under optical excitation, most of the excited electrons in ZnO were trapped by the defect states through a nonradiative decay process. The UV emission at 397 nm is attributed to part of the electrons in defect states recombined with the holes in ground states, while the energy of the rest carriers was transferred to Yb^{3+} ions through the nonradiative ET process which results in the NIR emission corresponding to the $^2F_{5/2} \rightarrow {}^2F_{7/2}$ transition of Yb^{3+}. As for the presently studied materials, the combined factors of the ZnO QDs density, defect states trapping rate and ET efficiency from ZnO QDs to Yb^{3+} determine the intensity of NIR emission. It is expected that the increase in the density of trap centers and energy transfer rate will enhance the intensity of NIR emission of Yb^{3+} ions, which makes ZnO–SiO_2:Yb^{3+} hybrid materials more suitable for spectral conversion of solar spectrum.

4. Conclusions

In summary, intense NIR emission at around 1 μm of Yb^{3+} ions have been measured from ZnO–SiO_2:Yb^{3+} hybrid materials upon broadband UV light excitation. Codoping with Li^+ ions increased the near-infrared luminescence intensity around 1 μm about twice at room temperature. Efficient ET from ZnO QDs to Yb^{3+} ions has been clarified by the systematic measurements and analysis of static and time resolved PL spectra. The development of ZnO–SiO_2:Yb^{3+} hybrid luminescent materials could open up a potential possibility in realizing high efficiency silicon-based solar-cells by converting the UV-blue part of the solar spectrum to NIR photons.

Acknowledgments

This work was supported by NSFC (50872036), Ph.D. Programs Foundation of Ministry of Education of China (20100172110012), and the Fundamental Research Funds for the Central Universities, SCUT. The authors would like to thank the support of China Scholarship Council (CSC). Support from the Singapore Ministry of Education through the Academic Research Fund (Tier 1) under Project No. RG40/07 and from the Singapore National Research Foundation through the Competitive Research Programme (CRP) under Project No. NRF-CRP5-2009-04 is gratefully acknowledged.

References

[1] P. Chen, M. Zhu, Mater. Today 11 (2008) 36.
[2] O. Guilatt, B. Apter, U. Efron, Opt. Lett. 35 (2010) 1139.
[3] B.M. van der Ende, L. Aarts, A. Meijerink, Adv. Mater. 21 (2009) 3073.
[4] D.C. Yu, S. Ye, M.Y. Peng, Q.Y. Zhang, J.R. Qiu, J. Wang, L. Wondraczek, Sol. Energy Mater. Sol. Cells 95 (2011) 1590.
[5] Q.Y. Zhang, X.Y. Huang, Prog. Mater. Sci. 55 (2010) 353.
[6] P. Vergeer, T.J.H. Vlugt, M.H.F. Kox, M.I. den Hertog, J. van der Eerden, A. Meijerink, Phys. Rev. B 71 (2005) 014119.
[7] X.Y. Huang, Q.Y. Zhang, J. Appl. Phys. 105 (2009) 053521.
[8] X.P. Chen, X.Y. Huang, Q.Y. Zhang, J. Appl. Phys. 106 (2009) 063518.
[9] L.C. Xie, Y.H. Wang, H.J. Zhang, Appl. Phys. Lett. 94 (2009) 061905.
[10] H. Lin, D.Q. Chen, Y.L. Yu, Z.F. Shan, P. Huang, Y.S. Wang, J. Alloys Compd. 509 (2011) 3363.
[11] B.C. Cheng, X.M. Yu, H.J. Liu, M. Fang, L.D. Zhang, J. Appl. Phys. 105 (2009) 014311.
[12] S. Ye, N. Jiang, F. He, X. Liu, B. Zhu, Y. Teng, J.R. Qiu, Opt. Express 18 (2010) 639.
[13] O.M. Ntwaeaborwa, P.H. Holloway, Nanotechnology 16 (2005) 865.
[14] X.P. Chen, F. Xiao, S. Ye, X.Y. Huang, G.P. Dong, Q.Y. Zhang, J. Alloys Compd. 509 (2011) 1355.
[15] Y.P. Du, Y.W. Zhang, L.D. Sun, C.H. Yan, J. Phys. Chem. C 112 (2008) 12234.
[16] X.Y. Zeng, J.L. Yuan, Z.Y. Wang, L. Zhang, Adv. Mater. 19 (2007) 4510.
[17] S. Panigrahi, A. Bera, D. Basak, ACS Appl. Mater. Interfaces 1 (2009) 2408.
[18] M. Bouguerra, M. Samah, M.A. Belkhir, A. Chergui, L. Gerbous, G. Nouet, D. Chateigner, R. Madelon, Chem. Phys. Lett. 425 (2006) 77.
[19] Z.P. Fu, B.F. Yang, L. Li, W.W. Dong, C. Jia, W. Wu, J. Phys.: Condens. Matter 15 (2003) 2867.
[20] W.H. Zhang, J.L. Shi, L.Z. Wang, D.S. Yan, Chem. Mater. 12 (2000) 1408.
[21] H.B. Zeng, G.T. Duan, Y. Li, S.K. Yang, X.X. Xu, W.P. Cai, Adv. Funct. Mater. 20 (2010) 561.
[22] K.W. Liu, R. Chen, G.Z. Xing, T. Wu, H.D. Sun, Appl. Phys. Lett. 96 (2010) 023111.
[23] X.T. Wei, S. Huang, Y.H. Chen, C.X. Guo, M. Yin, W. Xu, J. Appl. Phys. 107 (2010) 103107.
[24] Z. Zhou, T. Komori, T. Ayukawa, H. Yukawa, M. Morinaga, A. Koizumi, Y. Takeda, Appl. Phys. Lett. 87 (2005) 091109.
[25] C.H. Huang, T.M. Chen, W.R. Liu, Y.C. Chiu, Y.T. Yeh, S.M. Jang, ACS Appl. Mater. Interfaces 2 (2010) 259.
[26] Y.G. Su, L.P. Li, G.S. Li, Chem. Mater. 20 (2008) 6060.
[27] N. Jiang, S. Ye, J.R. Qiu, Appl. Phys. Lett. 108 (2010) 083535.